Ultra-High Performance Concrete Compression and Fracture Response Parameters for Lattice Discrete Particle Model Simulations

By

Rafic G. El-Helou[1], Erol Lale[2], Gianluca Cusatis[3], and Cristopher D. Moen[4]

[1]Ph.D. Candidate, The Charles E. Via, Jr. Department of Civil and Environmental Engineering, Virginia Tech, Blacksburg, VA 24060, USA. E-mail: relhelou@vt.edu

[2]Postdoctoral Research Fellow, Department of Civil and Environmental Engineering, Northwestern University, Evanston, IL 60208, USA. E-mail: lale@itu.edu.tr

[3]Associate Professor, Department of Civil and Environmental Engineering, Northwestern University, Evanston, IL 60208, USA. E-mail: g-cusatis@northwestern.edu

[4]Associate Professor, The Charles E. Via, Jr. Department of Civil and Environmental Engineering, Virginia Tech, Blacksburg, VA 24060, USA. E-mail: cmoen@vt.edu

Abstract: Lattice Discrete Particle Model (LDPM) simulation parameters are obtained for Lafarge Ductal Ultra-High Performance Concrete (UHPC) from unconfined compression, fracture, and direct tension tests. The LDPM predicts macroscopic behavior of concrete including compression, shear, and flexure limit states, through mesoscale constitutive relationships. The volume and orientation of fibers were considered as test variables. The experimental results showed a 7% increase in the ultimate compression strength when fibers, 2% by volume, were introduced in the UHPC matrix. The post-peak load carrying capacity also improved where the material maintained 50% of its ultimate carrying capacity at an axial strain 157% greater than the ultimate strain with a 4% fiber volume content. In the fracture tests, the peak load increased by a factor of 5 with the inclusion of 2% fibers by volume and by a factor of 6 when these fibers were oriented perpendicular to the crack plane. The post-peak loads also improved with increasing fiber content. LDPM parameters were obtained by simulating the material tests relevant to plain UHPC (without fiber reinforcement) and comparing the results to experimental data. The simulations will be coupled with fiber-pullout models to validate the model predictive capabilities for fiber-reinforced UHPC in support of a larger research effort to bring simulation-based analysis and design to concrete codes and standards.

Keywords: UHPC, LDPM, Fracture, Compression, Tension, Fibers, Material Characterization

1. Introduction and Research Vision

Structural-scale computational modeling of concrete components and systems including random cracking, failure patterns, and the influence of discrete fiber reinforcement is now possible because of advances in mechanics, numerical methods, and computational tools. The Lattice Discrete Particle Model (LDPM), for example, predicts the macroscopic behavior of Ultra-High Performance Concrete (UHPC) including compression, shear, and flexure limit states, through mesoscale constitutive relationships (Cusatis et al. 2011a, Schauffert and Cusatis 2011a). This formulation is chosen for the current study for its ability to predict concrete failure modes and crack patterns including the effect of aggregate size, discrete cracking, and fiber-matrix interaction.

UHPC is a high-strength material with a compressive strength exceeding 150 MPa, achieved when discrete steel fibers are combined with an optimized packing of cement, silica fume, fine sand, and water (Graybeal 2006). The fibers improve the durability and ductility of the composite by contributing to the resistance to tensile stresses, bridging crack surfaces, and limiting crack propagation (Lin and Li 1997, Lepech and Li, 2009; Wille and Naaman, 2012). When compared to conventional concrete, UHPC has a higher compressive strength with post-peak capacity, a higher tensile strength with enhanced ductility, and increased durability making it a superior alternative for many structural applications (Graybeal 2013). However, efforts made by the government and industry for its broad implementation into civil infrastructure is taking time to catalyze, in large part because design guides and computational tools for analyzing UHPC structural components are yet to be developed.

Concrete design equations and failure patterns have been traditionally investigated through experimental programs directed to specific structural applications. Experimental tests produce reliable data but are expensive, time consuming, and not feasible for exploration of a large number of variables. The LDPM provide an analysis-based alternative to tests that can accelerate the design and implementation of state-of-the-art innovative construction materials into civil infrastructure. However, predictive structural-scale UHPC computational simulations depend on careful material characterization that captures the material response in compression, tension, and fracture, and adequately describes interfacial properties between fibers and surrounding matrix. The research summarized herein contributes to this characterization by describing UHPC unconfined compression and fracture responses including post-peak behavior dependent on fiber content and orientation effect.

An experimental program is designed and implemented that builds on previous research to bring UHPC material characterization to structural-scale computational modeling. The tests quantify the direct tension strength, the axial and circumferential stress-strain response of unconfined UHPC in compression, and the fracture behavior for different fiber contents and orientation. The details of the computational modeling framework and the experimental program carried out for this research, including the test matrix, are introduced in the next sections.

2. Lattice Discrete Particle Model

The LDPM simulates concrete as a two-phase material composed of coarse aggregate grains held together by an embedded cementitious matrix. The mesostructure is constructed by randomly generating the aggregate centers and diameters, whose shapes are approximated as spheres, based on an assumed particle density function (Figure 1a). Zero-radius nodes are randomly generated over the model surface to create its external geometry. A Delaunay tetrahedralization connect the aggregate centers, and a 3D domain tessellation defines the particle interfaces and creates a system of polyhedral cells, each containing an aggregate and its surrounding matrix

(Figure 1b). These cells interact with each other through triangular facets which are also assumed to be potential crack surfaces (Figure 1a and 1c). To ensure that shear interaction between adjacent particles does not depend on the shear orientation, a vectorial constitutive law is imposed at the centroid of the projection of each single facet (contact point) onto a plane orthogonal to the straight line connecting the particle centers (lattice strut). The straight lines connecting the particle centers define the lattice system (Figure 1c).

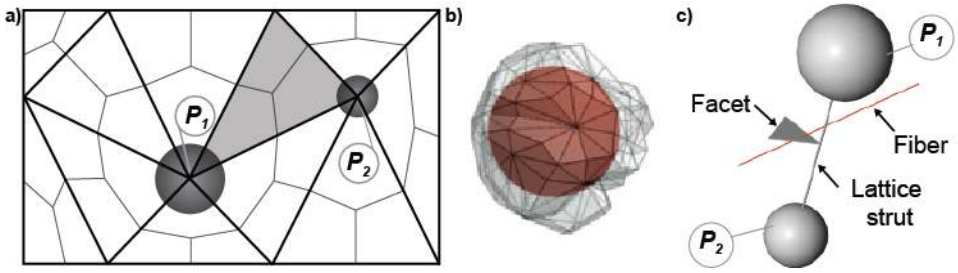

Figure 1: a) Two-dimensional mesostructure tessellation; b) Three-dimensional discrete particle; c) Facet intersecting a discrete fiber (El-Helou, 2014; Schauffert and Cusatis, 2012a)

The displacement field along the lattice struts and the displacement jump, $[\boldsymbol{u_c}]$, at the centroid of each facet are described through rigid body kinematics. The components of the strain vector in a local system of reference (normal and shear strains) are defined by the displacement jump at the contact point divided by the inter-particle distance, ℓ: $\varepsilon_N = \boldsymbol{n}^T[u_c]/\ell$; $\boldsymbol{\varepsilon_M} = \boldsymbol{m}^T[u_c]/\ell$; $\varepsilon_L = \boldsymbol{l}^T[u_c]/\ell$, where $\boldsymbol{n}$ is a unit vector orthogonal to the projected facet and $\boldsymbol{m}$ and $\boldsymbol{l}$ are mutually orthogonal unit vectors and lie in the projected facet. Equilibrium is imposed using the principle of virtual work by summing all the facet contributions and equating total internal and external work to obtain the discrete equilibrium equations of the LDPM formulation.

The elastic behavior is described by assuming that the normal and shear stresses are proportional to the corresponding strains: $\sigma_N = E_N\varepsilon_N$; $\sigma_M = E_T\varepsilon_N$; $\sigma_L = E_T\varepsilon_L$, where $E_N = E_0$, $E_T = \alpha E_0$, in which E_0 is the effective normal modulus of elasticity, and α is the shear-normal coupling parameter. The parameters E_0 and α are assumed to be material properties and are related to the macroscopic properties (modulus of elasticity, E, and Poisson's ratio, ν).

Beyond the elastic regime, the inelastic behavior is represented by three physical mechanisms including fracture and cohesion in tension and tension-shear, pore collapse and compaction in compression, and frictional behavior due to compression-shear. A detailed description of model behavior in the nonlinear range can be found in Cusatis et al., 2011a, and Cusatis et al., 2011b.

Schauffert and Cusatis (2012a, 2012b) extended the LDPM formulation to incorporate the effect of discrete short circular straight fiber reinforcement on the concrete behavior. The fiber formulation retains the discrete nature of the model generating all the fibers in a given concrete volume (random or preferred orientation) and overlapping it with the cell system of the LDPM as shown in Figure 1c. The LDPM fiber-matrix interaction formulation takes into account fiber pullout resistance considering debonding and frictional slip, matrix spalling, and fiber snubbing phenomena. The current LDPM formulation is implemented in MARS, a multi-purpose computational code for the explicit dynamic simulation of structural performance (Pelessone, 2016).

This paper obtains the LDPM parameters for Ductal UHPC governing compression, tension, and fracture behavior, namely, normal modulus E_0, alpha α, facet tensile strength σ_t, tensile characteristic length l_t, shear strength ratio σ_s/σ_t, initial friction μ_0, and softening

exponent n_t, through experimental testing. The details of the experimental investigation, including the test matrix, are introduced in the next section.

3. Experimental Program

The experimental program comprised of a total of 31 unconfined compression testing cylinders, 43 direct tension dogbone-shaped specimens, and 37 three-point bending (notched) fracture toughness prisms. The UHPC used in these tests is commercially available, called Ductal, and is supplied in the form of a dry premix powder, water, superplasticizer, and steel fibers. A typical UHPC composition of Ductal with 2% fiber volume content (v = 2%) can be found in Graybeal (2006). The fibers are smooth high carbon steel with a nominal length of 13 mm and a diameter of 0.2 mm.

3.1 Test Matrix

The compression, tension, and fracture behavior of UHPC was evaluated without fiber reinforcement (v = 0%) and with fibers added as a percentage of the total mix volume (v = 2%, 4%). A key parameter to UHPC material response is fiber orientation as it influences crack initiation and propagation, and it was varied by placing UHPC randomly or from one side of the molds, allowing the concrete to flow to the other side as it fills the mold volume. After placement, the specimens were covered with plastic sheets and left to cure at room temperature for 48 hours. Table 1 shows the details of the test matrix.

Table 1: Experimental Test Matrix

Batch ID	v (%)	Tests Performed	Placement Method	Tested Specimens
I, II	0	Unconfined Compression	N/A	9
		Fracture toughness	N/A	12
		Direct Tension	N/A	20
III	2	Unconfined Compression	N/A	12
		Fracture toughness	Random	5
		Direct Tension	N/A	12
IV	2	Fracture toughness	One side	6
V	4	Unconfined Compression	N/A	10
		Fracture toughness	Random	6
		Direct tension	N/A	11
VI	4	Fracture toughness	One Side	8

3.2 Unconfined Compression

The compression specimens were placed in cylinder molds having a diameter of 76 mm and height of 165 mm. The molds are made of 7 mm thick plastic to ensure rigidity and to prevent the deformation due to the pressure of fresh concrete (Figure 2a). The top 13 mm of the cylinders were cut using a diamond blade saw to obtain clean smooth top surfaces. The surfaces were then manually grinded and the planeness was measured using a flat steel plate and a dial gage. The final specimens had a diameter of 72 mm and a height of 102 mm with an end planeness less than 1 degree as recommended by Graybeal (2016). The tests were performed using a SATEC 1,334-kN capacity compression machine. An averaging axial extensometer (Epsilon 3542) with 6 mm range was mounted over a 50-mm gauge length at the middle of the cylinder to measure the axial displacement and to avoid end effects. The total displacement was measured using two Linear Variable Differential Transformers (Vishay HS10 LVDT), with 13 mm range, mounted

between the machine platform and top metal socket. The circumferential expansion was recorded using a circumferential extensometer (Epsilon 3544) connected to a chain device mounted around the circumference at mid-height of the cylinder as shown in Figure 2b. To avoid erroneous data at the beginning of each test because of platen seating and cylinder surface irregularities, a preload of 4 MPa was applied prior to the start of each test and the pre-cracking axial displacements were measured using the axial extensometer mounted directly on the cylinder. After cracking, the axial extensometer moved and its data was no longer reliable. The LVDTs' data was used beyond cracking after correcting the pre-cracking LVDT data to coincide with the axial extensometer readings eliminating the testing-frame deformation and concrete-steel frictional end effects.

Figure 2: a) Cylinder UHPC placement; b) Unconfined compression test setup with ν = 2 %

The compression-testing procedure was in accordance with ASTM C39/C39M with one exception: the tests were displacement-controlled with a constant circumferential displacement rate of 2.1×10^{-4} mm/s until the peak axial stress was reached, after which the displacement rate was increased to 2.5×10^{-3} mm/s and 8.5×10^{-3} mm/s, respectively. This displacement rate was selected after a series of trial-and-error tests to find the loading scheme that captures best the elastic and post-peak portions of the stress–strain compressive curve while keeping the test duration below 20 min to avoid long-term effects. The adopted pre-peak circumferential displacement rate corresponds to an average load rate of 0.42 MPa/s. The compression specimens were tested between 400 to 410 days from UHPC placement.

3.3 Fracture Toughness

The fracture specimens were placed in specially designed Polyvinyl chloride (PVC) molds having a width of 51 mm, a height of 115 mm, and a length of 508 mm. The molds are made of 25 mm thick PVC to ensure rigidity of the form, to prevent deformations, and to facilitate demolding without using form oil. The specimens were deliberately made 51 mm longer to provide extra length for the concrete to flow from one side to the other (Figure 3a). This placement technique is adopted in batches IV and V (Table 1) to align the fibers parallel to the specimen's bottom surface. The extra 51 mm where the concrete is placed is cut after demolding using a diamond saw. The top 13 mm of the specimen along with a 5 mm wide and 25 mm high round tip notch in the middle of the prism were cut using waterjet cutting technology. Waterjet cutting was used to ensure plane and parallel prism surfaces and to reduce geometric irregularities between the tested specimens. The final specimens had 51 mm width, 102 mm height, and 457 mm length.

The testing procedure was based on recommendations by Graybeal (2006), which is partially based on ASTM E1820. The tests were performed in an MTS compression machine with a 50 kN load cell as shown in Figure 3b. A clip-on gage (Epsilon 3541) with 8 mm range

was mounted to knife edges glued to the notch boundary to measure the crack mouth opening displacement (CMOD). The tests were displacement-controlled with a constant CMOD rate of 0.018 mm/s; the post-cracking rate was carried out about 3 to 5 times higher. The fracture specimens were tested 156 to 199 days after UHPC placement.

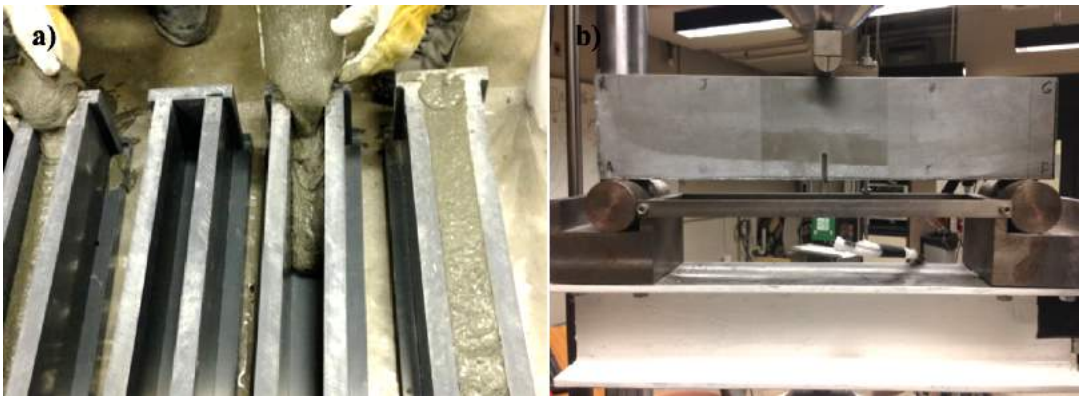

Figure 3: a) Concrete placed from one side (v = 4%); b) Fracture toughness test setup

3.4 Direct Tension

The direct tension specimens were placed in dogbone-shaped molds having a length of 76 mm, a depth of 25 mm, and a cross-sectional area of 645 mm^2 at midlength. The testing procedure was partially based on the cement mortar direct tension testing method described in AASHTO T132. The specimens were installed in an MTS tension machine with a 150 kN load cell and the tests were carried out displacement-controlled with a constant cross-head displacement rate of 0.025 mm/s (Graybeal 2006). The tension tests were performed 232 to 237 days after placement.

4. Results and Discussion

4.1 UHPC Unconfined Compression Behavior

The individual compression axial stress - axial strain curve of each tested cylinder without fiber reinforcement (v = 0%) and with 4% fiber volume content including the post-peak behavior are shown in Figure 4; the average trends are plotted as thicker solid lines. The average curve is calculated from the individual axial stresses at one value of axial or circumferential strain. Unlike fiber-reinforced UHPC, obtaining the post-peak response of the specimens without fibers was challenging due to the explosive nature of the failure and the material's high sensitivity to a slight increase in load around the peak load as multiple cracks developped (Figure 4a). Figure 5 shows the average axial stress versus axial and circumferential curves for UHPC with v = 0%, 2%, and 4%.

The axial stress - axial strain initial stiffness for UHPC with and without fibers was similar, approximately 53.7 GPa; it begins to degrade when microcracks develops resulting in a non-linear behavior as the load approaches the peak stress. The ultimate compressive strength of UHPC without fibers is 139 MPa and then it increases to 155 MPa and 157 MPa when fibers 2% and 4% by volume are added to the matrix. Fibers improved the ductility of the material by transmitting forces between crack surfaces maintaining confinement and limiting crack initiation and propagation as shown in Figure 5. For example, the material was able to withstand 50% of its ultimate capacity at axial strains of 0.006 and 0.009 when fibers are added at 2% and 4% by volume, respectively.

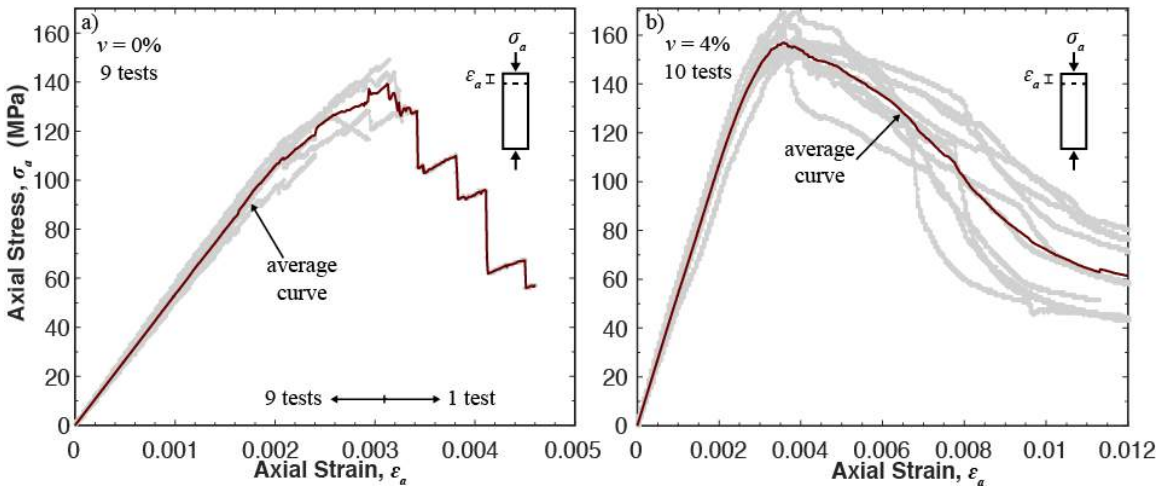

Figure 4: Individual and average compression axial stress – axial strain response for UHPC with a) no fiber and b) 4% fiber volume content

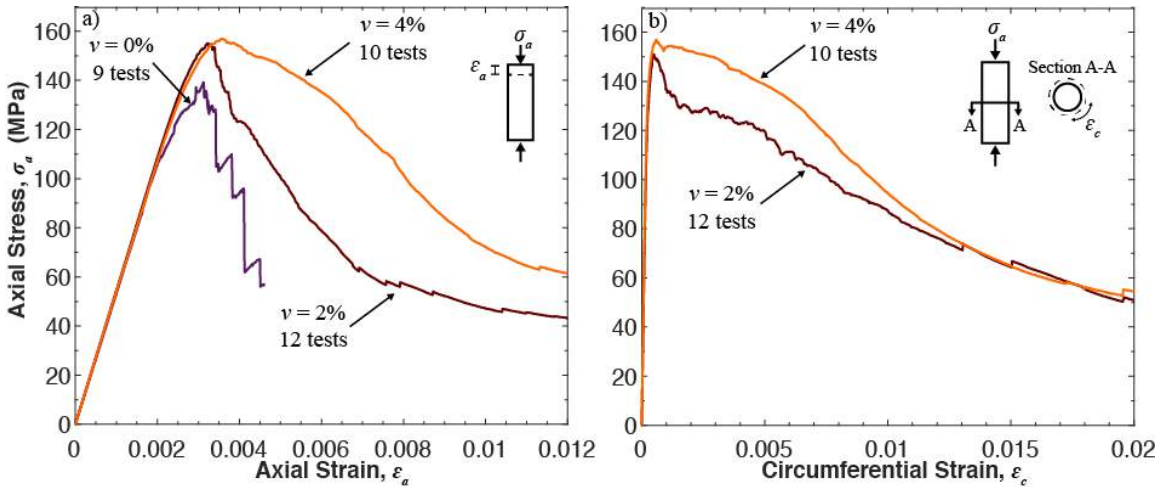

Figure 5: Average UHPC compression behavior at different volume contents: a) axial stress – axial strain curve; b) axial stress – circumferential strain

4.2 UHPC Fracture Behavior

The individual trends for the fracture toughness tests with 2% fiber volume placed from one side of the specimen (Figure 3a) are shown in Figure 6a, with the average response plotted with a thicker solid line. Figure 6b shows the average load – CMOD curves for all fracture specimens with different fiber reinforcement ratios and placement methods. The crack propagation during the tests was well controlled and the post-peak response was captured for UHPC with and without fibers. The unreinforced specimens split in two equal pieces at the end of each test at an average crack opening of 0.83 mm while the fiber reinforced specimen tests were stopped at a crack displacement of 3 mm without complete failure.

The average peak load of the unreinforced specimens is 2.0 kN and it increased to 10.4 kN when 2% fibers by volume were added. When fresh concrete with v = 2% flowed from one side of the prism to the other, fibers were preferentially aligned parallel to the bottom side of the mold and perpendicular to the cracking plane, resulting in efficient crack control which increased the peak load to 12.5 kN (20% of peak load compared to the random placement method). The peak load further increased to 17.5 kN when fresh UHPC was randomly placed at higher fiber volume (v = 4%), which resulted in a larger number of fibers bridging the cracks. However,

placing fresh concrete from one side with v = 4% reduced the fracture peak load to 15.7 kN (10% decrease compared to random placement). It is hypothesized that with higher fiber volume content, chunks of fibers are formed as the concrete is flowing which disturbed fiber alignment. It should also be noted that Ductal UHPC mix was optimized for 2% fibers to ensure adequate flowability of wet concrete, which could also explain the formation of fiber chunks observed during placement. X-Ray CT scans are planned to calculate the amount of the fibers aligned in each direction, which is a key parameter in the LDPM simulations for fiber-reinforced concretes.

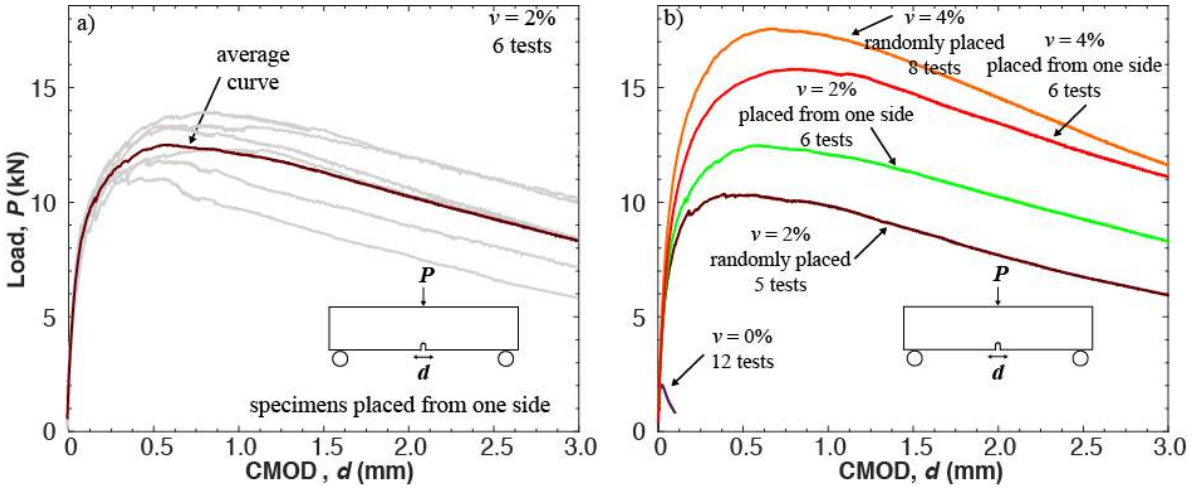

Figure 6: UHPC load - CMOD fracture curves for a) v = 2% with concrete placed from one side and b) different volume contents and placement methods

4.3 UHPC Direct Tension Strength

The average direct tensile strength for plain UHPC (v = 0%) was 8.5 MPa. The inclusion of fibers at v = 2% marginally decreased the tension capacity to 7.9 MPa. Fibers at v = 4% efficiently bridged the formed microcracks providing resistance to tensile stresses and increased the tension capacity to 12.5 MPa. In both series of fiber-reinforced UHPC tests, the specimens did not fail at peak strength and showed a post-peak response, which signify that the tension strength of UHPC could be considered in structural design reducing or eliminating tension reinforcement. The tension stress-strain curve was not generated because an axial extensometer to read displacements was not mounted directly on the specimen.

5. LDPM Parameter Identification for Ductal UHPC

The LDPM constitutive equations at the facet level depend on a number of parameters that are obtained from material tests. In this paper, the simulation models for compression, tension, and fracture tests were built to mimic the experimental conditions including dimensions, loading, and support boundary conditions (Fig. 7). The mix proportion parameters necessary to construct the LDPM mesostructure was determined based on a typical Ductal UHPC mix composition (Graybeal, 2006) with a cement content c = 712 kg/m^3, water-to-cement-ratio w/c = 0.15, aggregate-to-cement-ratio a/c = 1.43, and fuller coefficient n_F = 0.5. A coarse-grained approximation technique was adopted to decrease computational cost (Smith et al., 2014) and thus, the UHPC minimum aggregate size, d_0, was increased to 2 mm and capped at d_a = 4 mm. This technique is based on the observation that particle size does not influence LDPM macroscopic response for the UHPC in consideration (Smith et al., 2014). The model elastic parameters, E_0 = 90 GPa and α = 0.292, were first calibrated by using the elastic formulas

(reported in Cusatis et al., 2011a); The matching of the numerical stress-strain curve and the experimental modulus of elasticity (E = 53.7 GPa) is shown in Fig. 7a.

The facet tensile strength, σ_t = 7.5 MPa, and tensile characteristics length, l_t = 50 mm, were obtained by comparing the simulated macroscopic results of the direct tension and fracture toughness tests to the experimental data. The simulated macroscopic tensile strength of plain UHPC was 8.1 MPa which is in good agreement with the experimental results (8.5 MPa). The model's load-CMOD curve for the fracture test is plotted with respect to the experimental data in Fig. 7b. The simulated maximum fracture load was higher than the experimental load because the adopted coarse graining approximation changes the accuracy of the stress concentration at the notch tip, which in turn influences the shape of the load-CMOD curve at the peak load. A key advantage in the LDPM simulations is the model's ability to capture the fracture failure mode through the visualization of the crack initiation and propagation in middle of the specimen as is shown in Fig. 7b.

The nonlinear portion of the compressive stress-strain curve (Fig. 7a) was captured by setting the shear strength ratio σ_s/σ_t at 8.5, and initial friction μ_0 at 0.15. The softening exponent $n_t = 0.2$ was found to properly simulate the post-peak response. Fig. 7a also shows the LDPM ability to capture the compression failure mode through the generation of splitting cracks as the load reaches failure.

Finally, properly capturing the LDPM parameters requires identification of the material parameters governing fiber-matrix interaction, which is ongoing research of the authors to validate the formulation for UHPC with fiber reinforcement and is left for future publications.

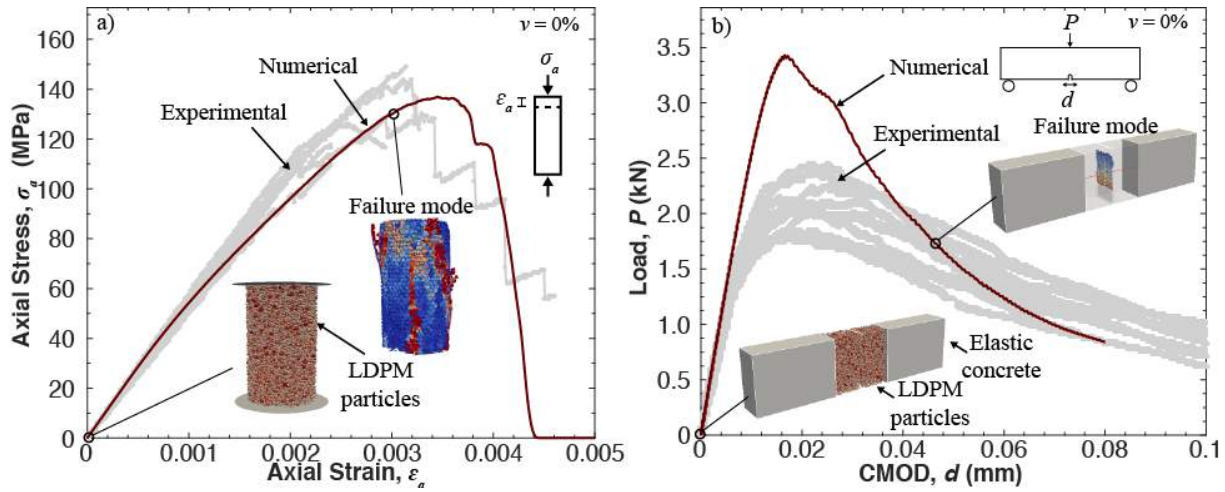

Figure 7: Numerical results and failure modes for LDPM parametric identification with ν = 0% for a) unconfined compression and b) fracture toughness

6. Conclusions

An experimental investigation was conducted to obtain UHPC compression, tension, and fracture behavior for use in UHPC computational models. LDPM input parameters for compression and tension of UHPC were obtained and compared to experimental data. The experimental investigation showed the effects of the content and orientation of fibers on the material behavior, which is as a key parameter in any computational model. The numerical results, including failure modes and crack patterns, were in good agreement with the experimental data. The predictive capability of the LDPM will be validated in the near future for fiber-reinforced UHPC by coupling the parameters with fiber pullout models in support of a larger research effort to bring simulation-based analysis and design to concrete codes and standards.

7. Acknowledgements

This study is based upon work supported by the National Science Foundation under Grant No. 1201087 to Virginia Tech with Subcontract to Northwestern University. The authors acknowledge the support of LaFarge Ductal for providing the materials free of charge. Special thanks to Dr. Roman Wendner for his help with the material test setup design and procedure. The authors would like to also acknowledge the faculty and staff of Virginia Tech Structural and Mechanics laboratories namely Dr. David Mokarrem, Mac McCord, Brett Farmer, and Dennis Huffman. Special thanks to Valerie Black, Thomas Dacanay, and Rachel Gordon for their help with UHPC mixing, placing, and the execution of the tests. The opinions, findings, and conclusions or recommendations expressed in this paper are those of the authors and do not necessarily reflect the views of the sponsors.

8. References

AASHTO T132, "Standard Method of Test for Tensile Strength of Hydraulic Cement Mortars Standard". *American Association of State Highway and Transportation Officials*. 2013.

ASTM C39/C39M, "Standard Test Method for Compressive Strength of Cylindrical Concrete Specimens," *American Society for Testing and Materials Standard International*. West Conshohocken, PA, 2016.

ASTM E1018, "Standard Test Method for Flexural Toughness and First-Crack Strength of Fiber-Reinforced Concrete (Using Beam With Third-Point Loading)," *American Society for Testing and Materials Standard International*. West Conshohocken, PA, 1997.

Cusatis G., Mencarelli A., Pelessone D., Baylot J. "Lattice Discrete Particle Model (LDPM) for failure behavior of concrete. II: Calibration and validation". *Cement and Concrete Composites*. 2011; 33(9):891-905.

Cusatis G., Pelessone D., Mencarelli A. "Lattice Discrete Particle Model (LDPM) for failure behavior of concrete. I: Theory". *Cement and Concrete Composites*. 2011; 33(9):881-890.

El-Helou, R.G., Lale, E., Moen, C.D., and Cusatis, G. (2014), "Lattice discrete particle modeling of buckling deformation in thin ultra-high-performance fiber-reinforced concrete plates", *Computational Modelling of Concrete and Concrete Structures Conference (EURO-C 2014),* March 24-27, 2014, St. Anton am Alberg, Austria.

Graybeal B.A. "Material Property Characterization of Ultra-High Performance Concrete." *Federal Highway Administration*, U.S. Department of Transportation, Report No. FHWA-HRT-06-103, 2006.

Graybeal B.A. "Ultra-High Performance Concrete: A State-of-the-Art Report for the Bridge Community." *Federal Highway Administration*, U.S. Department of Transportation, Report No. FHWA-HRT-13-060, 2013.

Lepech M.D., Li V.C. "Water permeability of engineered cementitious composites". *Cement and*

Concrete Composites. 2009; 31(10):744-753.

Lin Z., Li V.C. "Crack bridging in fiber reinforced cementitious composites with slip-hardening interfaces". *Journal of the Mechanics and Physics of Solids*. 1997; 45(5):763-787.

Pelessone D., "Modeling and analysis of the response of structures". *User's manual*, ES3 Inc. 2016.

Schauffert E.A., Cusatis G. "Lattice Discrete Particle Model for Fiber-Reinforced Concrete. I: Theory". *Journal of Engineering Mechanics*. July 2012.

Schauffert E.A., Cusatis G., Pelessone D., O'Daniel J.L., Baylot J.T. "Lattice Discrete Particle Model for Fiber-Reinforced Concrete. II: Tensile Fracture and Multiaxial Loading Behavior". *Journal of Engineering Mechanics*. 2012; 138(7):834-841.

Smith, J., Cusatis, J., Pelessone, D., Landis, E., O'Daniel, J., and Baylot, J. "Discrete modeling of ultra-high-performance concrete with application to projectile penetration". *International Journal of Impact Engineering*, 2014; 65: 13–32.

Wille K., Naaman A.E. "Pullout Behavior of High-Strength Steel Fibers Embedded in Ultra-High-Performance Concrete". *Materials Journal*. 2012; 109(4):479-488.